Journal of Visualization, Vol. 4, No. 4 (2001) 331-339

Flow Visualization of a Longitudinal Vortex in Drag-reducing Surfactant Flow

Eschenbacher, J. F.* , Nakabe, K.* and Suzuki, K.*

* Department of Mechanical Engineering, Kyoto University, Kyoto 606-8501, Japan.

Received 7 March 2001.
Revised 31 July 2001.

***Abstract*:** Vortical structures behind a wing-type vortex generator (WVG) immersed in a drag-reducing flow were visualized with a fluorescence dye illuminated with a planer laser sheet to investigate the enhancement mechanism of heat transfer on the WVG-installed target wall. Particle image velocimetry (PIV) system was also used to measure the flow velocity profiles. Both the flow visualization and the velocity measurement revealed that small amounts of surfactant, Cetyl-Trimethyl-Ammonium-Chloride/ Sodium Salicylate (CTAC/NaSal), added in water changed drastically the flow patterns together with the wall heat transfer distributions due to the reduction of momentum exchange in the vortical flows behind WVG.

***Keywords*:** drag-reducing flow, vortex generator, longitudinal vortex, flow visualization, dye injection, PIV.

1. Introduction

Many heat transfer enhancement devices as turbulence promoters, surface renewal variations and other geometrical modifications were examined and reported in literature so far. These conventional devices applied to Newtonian fluids, however, may not fulfill appropriate functions of their performance in drag-reducing flows. Namely, in the case where small amounts of additives, for example, polymer, fiber or surfactant, were added to water, it was found that the coefficients of both turbulent wall friction and heat transfer were reduced down to around 20 percent of those of water (Gyr and Bewersdorff, 1995; Kawaguchi et al., 1997). For these diluted solutions, the specific properties of which are supposed to result in a dynamic internal alignment of molecules or micelles in nanometer order, it is difficult to establish suitable parameters to universally describe the flow and temperature fields. According to the results by Gyr and Bewersdorff (1995), highly damped turbulent mass and momentum transfers cause remarkable drag-reducing effects. Thus, well-known approximations such as Prandtl-von Karman's similarity hypothesis are not matched to the phenomena observed in surfactant flows anymore. Instead, new key factors such as Virk's maximum drag reduction asymptote (Virk et al., 1970) should be introduced to quantitatively describe the characteristics of drag-reducing flows.

In drag-reducing flows, the suppression of momentum exchange acts mainly normal to the main flow direction and leads to apparent flow laminarization in relatively lower flow velocity range up to a critical Reynolds number, where the pure solvent clearly flows in turbulent manner. Exceeding the value of the critical Reynolds number, or being subjected to the corresponding high shear rate, the drag-reducing solutions show similar drag and heat transfer characteristics as the pure solvent, that is, water in the present study. This recovery trend of drag-reducing flows was found to be irreversible for polymer or fiber solutions due to their one-way mechanical or thermal degradations. Thus, the drag reduction performance of polymer solutions will not be suitable in repeated use, for example, in a recirculating flow path with mechanical stresses by centrifugal pumps. Cationic surfactants

with counter ions, on the other hand, withstand and recover from the degradations caused by high shear rate or overloading heat flux. This could be caused by the shear-induced breakup and the shear-relaxed reproduction of the micelle network structures of surfactant aligned in flow direction (Kawaguchi et al., 1997). Depending on the local flow velocity, fluid temperature and surfactant concentration, locally high shear rates can exceed the maintaining forces of micelle alignment, destroy the drag reduction structure, and force the surfactant solution to obey the properties of the solvent. Thus, surfactants are considered to be one of the most appropriate drag-reducing additives for closed-loop thermal energy transport systems since they provide the advantage to keep their performance for a long time.

Now in time of increasing efforts for CO_2 emission reduction and energy saving, the addition of surfactants to the working fluid in long pipelines such as far-district heating/cooling systems seems to be very attractive to reduce pumping energy and heat loss through the pipe walls to the outside simultaneously. To apply this promising method to such engineering applications, however, the effects of drag reduction on flow and heat transfer characteristics have to be examined more in detail. So, it will be possible to find new methods to enhance the heat transfer locally in the heat exchangers at the terminals of the far-district heating/cooling systems with little additional efforts to reduce the size of the heat exchangers.

Since longitudinal vortices generated in forced convection flows show considerably good enhancement results of wall heat transfer with flow rotation and flow destabilization together, the present experimental study is concentrated on the visualization of the fluid motions with a longitudinal vortex generated behind a delta-shaped wing-type vortex generator (WVG) immersed in the surfactant solutions of several different concentrations; 0, 30, 100 and 200 ppm CTAC, together with the equimolar counter ion NaSal.

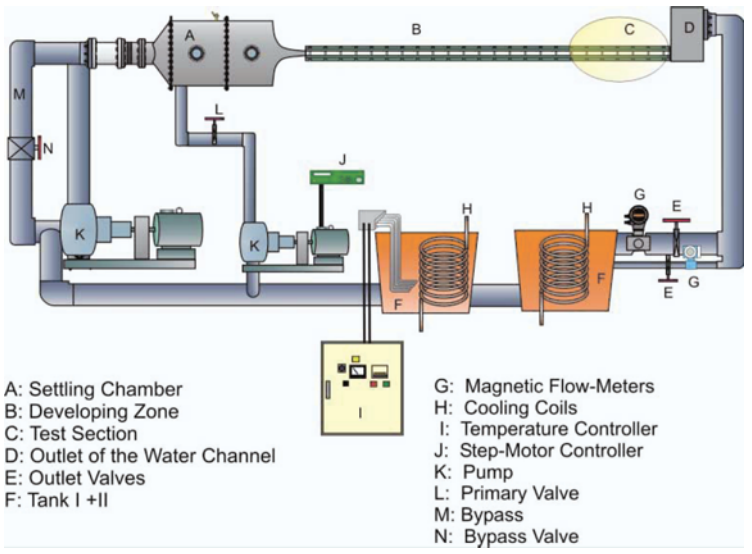

Fig. 1. Experimental apparatus.

2. Experimental Facilities and Methods

The experiments were carried out in a closed-loop rectangular water circuit as shown in Fig. 1. The working fluid in a pair of reservoir tanks ($1m^3$ each) connected in series was sucked by one of two centrifugal pumps and driven through a settling chamber into the test section of the duct, $W = 500$ mm wide and $H = 25$ mm high. The duct itself consists of an entrance region, $200H$ long, and the following test section, $40H$ long, made of acrylic plates to have an optical access through the duct wall.

The temperature of the fluid was precisely controlled within its fluctuation of ± 0.1K via a temperature regulator installed in the downstream tank. The mass flow rate was adjusted by main and bypass valves and monitored by two parallel magnetic flow meters installed downstream of the test section.

Figure 2 shows the geometry of the test section and the vortex generator, WVG, together with the coordinate system. WVG was made of brass and attached to the bottom surface of the test section. Its angle of attack against the main flow was fixed at 30 degrees. The height of the trailing edge was $0.5H$ and the base length

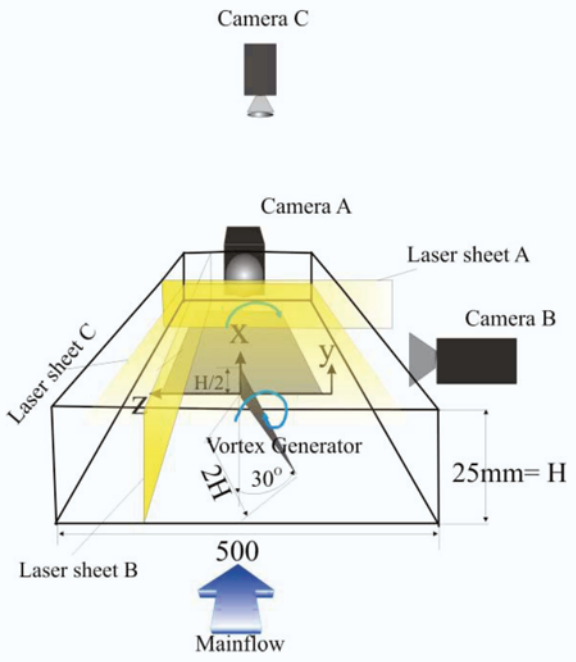

Fig. 2. Test section and optical arrangement.

was set equal to 2*H*, following Tiggelbeck et al. (1993). To conduct the flow visualization and develop the PIV measurements, the trailing surface of WVG was equipped with two holes for dye or tracer injection. Fluorescent dye, Uranine, injected through both holes was used as tracer to visualize the longitudinal vortices. Cross-sectional images of the injected dye illuminated by a planer Ar^+ laser were recorded with a digital home video camera. Small amounts of TiO_2 particles, 3 μm in average diameter, as tracer for the PIV measurements, were added to the main flow to obtain quantitative data of cross-sectional velocity profiles in the wake of WVG.

An illustration of the optical arrangement is also shown in Fig. 2. The y-z cross-sectional scattering images of the tracer particles illuminated by another planer laser of double-pulsed Nd:YAG were recorded in frame grabber memories through the cross-correlation CCD camera A, while the x-y and x-z cross-sectional images through the cameras B and C, respectively. The two-dimensional component vectors of flow velocity and their vorticities in y-z, x-y or x-z sections were estimated by cross-correlation coefficients calculated with a pair of particle image frames captured at 1.0 ms time interval by the cameras A, B or C. The averaged velocity maps shown in the following sections were arithmetically averaged over 30 individual vector maps.

3. Results and Discussion

3.1 Flow Visualization

To compare the vortical structures between 30 ppm CTAC/NaSal surfactant solution, (a) CTAC30, and tap water, (b) Water, the cross-sectional flow patterns were visualized in the x-y plane at $z/H = 0$ with laser sheet alignment B. In all images shown in Fig. 3, the trailing edge of WVG is situated at the left end of the image, and the main flow comes from the left to the right. The Reynolds number based on the duct height was kept constant at 4,000 (top image), 10,000 (middle image) and 20,000 (bottom image) in each case. The surfactant solution can exhibit the three different flow regimes, laminar, transitional and turbulent flows, in the present experimental conditions of the CTAC30 case since the critical Reynolds number in the same conditions without WVG was measured to be in the range of 6,000 ~ 10,000, dependent on the main flow temperature. It is clearly observed in the case of $Re = 4{,}000$ of pure solvent, (b) Water, that the flow already behaves in turbulent manner. The curl-up motions and large-scale turbulent vortices developing within a short distance behind the WVG were observed to rotate and entrain the fluid near the bottom wall. In the case of (a) CTAC30, on the contrary, under the same Reynolds number, $Re = 4{,}000$, only small-scale rotating fluid motion was observed, and the injected dye trajectory does not spread so much in the core region of the vortex. Thus, the flow behaves apparently laminarization with highly reduced turbulence in this surfactant case.

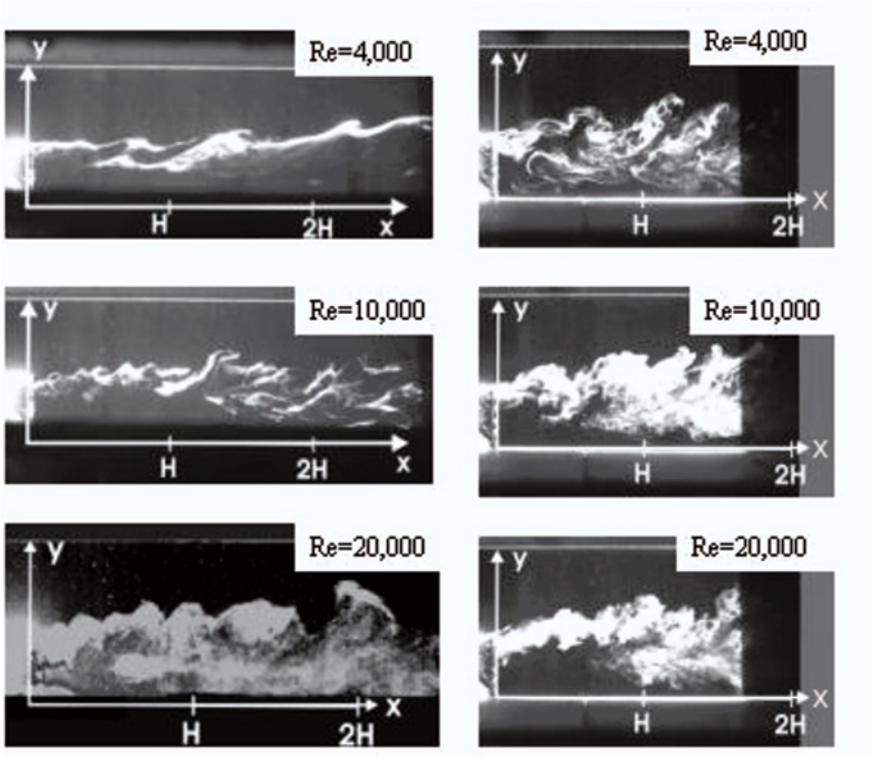

Fig. 3. Formation of longitudinal vortex behind WVG.

For the case of Re = 20,000, it is worth to mention that the difference of the flow patterns between (a) CTAC30 and (b) Water was apparently small, and that the flow structures in the wake behind WVG were similar to each other, in spite of relatively poor quality of the brightness and black and white contrast of the images. These results suggest that the alignment of the surfactant micelles to damp the turbulence (Toms effect) could be locally destroyed by higher shear rates due to large Reynolds number and intense rotation of the vortex, which causes the dye thread to quickly disperse into the working fluid. This local diminution of drag-reducing properties over the critical Reynolds number by the high flow velocity coincides well with the authors' previous heat transfer data (Eschenbacher et al., 1999). For the case of Re = 10,000, the visualized flow patterns demonstrate the transient trend in between the above-mentioned two Reynolds number cases.

3.2 PIV Measurements

Figures 4 and 5 show the cross-sectional velocity vector maps at the streamwise location, x/H = 2.5, in the cases of Reynolds numbers, 6,750 and 9,900, respectively. In each figure, (a) is the case of water and (b) the case of CTAC/NaSal 30 ppm (CTAC30). The orthogonal projection of WVG onto the y-z plane with laser sheet alignment A (cf. Fig. 2) was also drawn in each map. The main flow comes from the backside to the front of the page, facing to the upstream. It is obviously observed that a large-scale longitudinal vortex is generated downstream of the WVG. The comparison of these four vector maps reveals that the length-scale and intensity of the vortex depends on the solution concentration and the Reynolds number. If examined in more detail, it is found that the diameter of the vortex in the CTAC30 case has a relatively smaller than the one in the water case. Also, the center of the vortex core in CTAC30 is situated at a bit higher y/H position, compared with the water case. These results coincide with video images of the longitudinal vortex visualized in the above section. It can be explained that the exchange of turbulent momentum transfer between the vortex core and its vicinity is suppressed in the drag-reducing flow and then the growth of the vortex in the downstream is much slower than the water case.

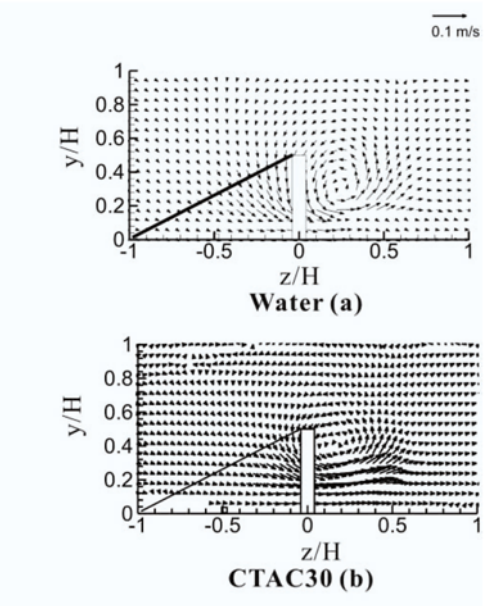

Fig. 4. Velocity vector maps in y-z cross-section ($x/H = 2.5$ and $Re = 6{,}750$).

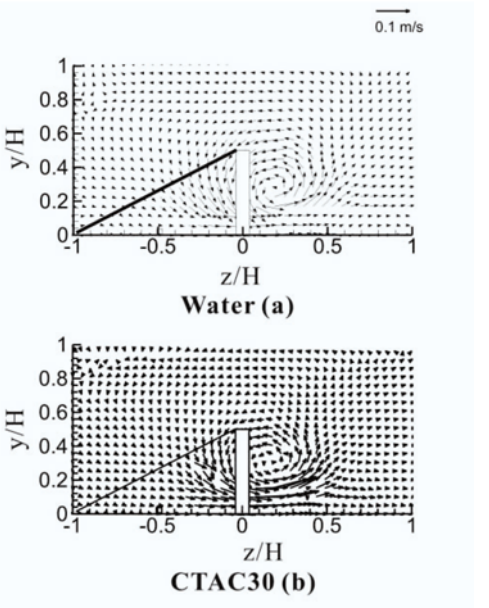

Fig. 5. Velocity vector maps in y-z cross-section ($x/H = 2.5$ and $Re = 9{,}900$).

Figure 6 shows the distributions of the cross-sectional velocity component vectors (u, v) and the contours of the speed S in the x-y plane at $z/H = 0$, obtained with laser sheet alignment B (cf. Fig. 2). The speed S is defined as below:

$$S = \sqrt{u^2 + v^2} \tag{1}$$

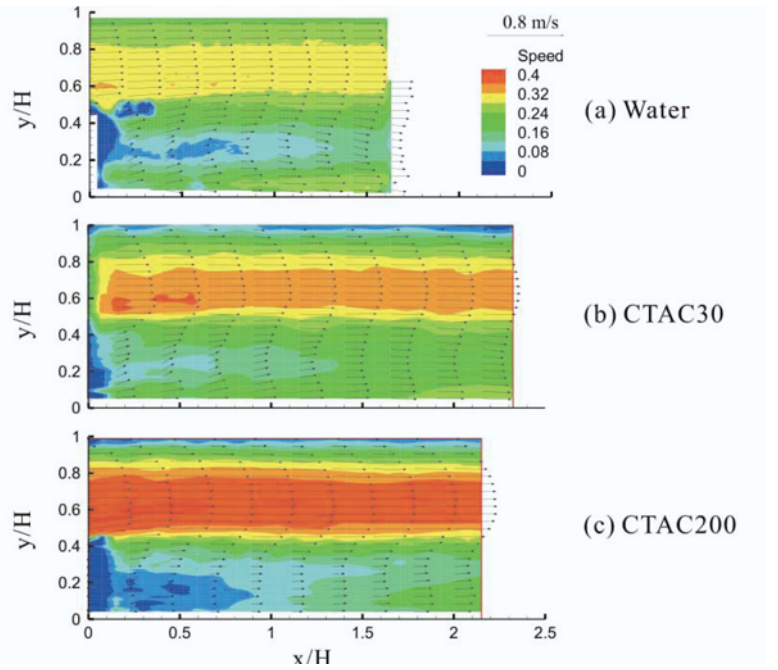

Fig. 6. Velocity vector maps in x-y cross-section ($Re = 9{,}900$ and $z/H = 0$).

The maps (a) Water, (b) CTAC30 and (c) CTAC200 in the figure correspond to three different concentration cases of surfactant, 0 ppm, 30 ppm and 200 ppm, respectively, under the same Reynolds number, Re = 9,900. The main flow direction of these maps is from the left to the right-hand side, and the trailing edge of the WVG is situated in the regions of y/H = 0 ~ 0.5 at x/H = 0. Relatively low speed regions are situated downstream of the WVG where the longitudinal vortex exists. Resulting in this flow deceleration, a high-speed region above the WVG, $y/H \geq 0.5$, was also clearly observed in all cases. The range of the low speed region expands more over the channel height with an increase in the concentration of the surfactant. Outstanding features of these maps are the fact that the wake region $y/H \leq 0.5$ of the water case shows larger velocity gradients than the other two cases, CTAC30 and CTAC200. This result of the water case is caused by high momentum exchange between the core and its vicinity. On the contrary, in the case of CTAC200, in particular, the streamwise velocities inside the generated vortex keep remarkably constant. The micelle structures may remain in the wake below the specific critical shear rates to suppress an added axial momentum through centrifugal forces, and then the vortex core can rotate like a rigid rod. The velocity gradient appears to have a maximum at the vortex boundary, where local shear stress exceeds the critical one, at $y/H \approx 0.5$. The case of CTAC30 solution may have a transient trend between drag-reducing flows and non drag-reducing ones since the outer regions of the vortex are significantly accelerated, compared to the CTAC200 case, but less than the water case. The high-speed region close to the bottom wall, x/H = 0.7 ~ 1.5, in this case corresponds to the heat transfer enhancement region (Eschenbacher et al., 1999).

The typical flow patterns of the CTAC30 case in the downstream region are shown in Fig. 7 under the drag reduction conditions; Re = 20,000 and T = 25℃. Here, the overall flow patterns behind the WVG are plotted in three-dimensional viewpoint. The colored contours represents local values of the speed S defined above. In this figure, it is clearly seen that high-speed regions are observed near the bottom wall throughout the measured regions of the wake behind WVG. The maximum value of the local high-speed spots is a bit above the bottom wall, and the rotational speed of the longitudinal vortex keeps over a long streamwise distance, which reveals again a suppressed momentum transfer between the vortex and its vicinity. The vortex path was observed, corresponding well to the distribution of high heat transfer rates previously observed.

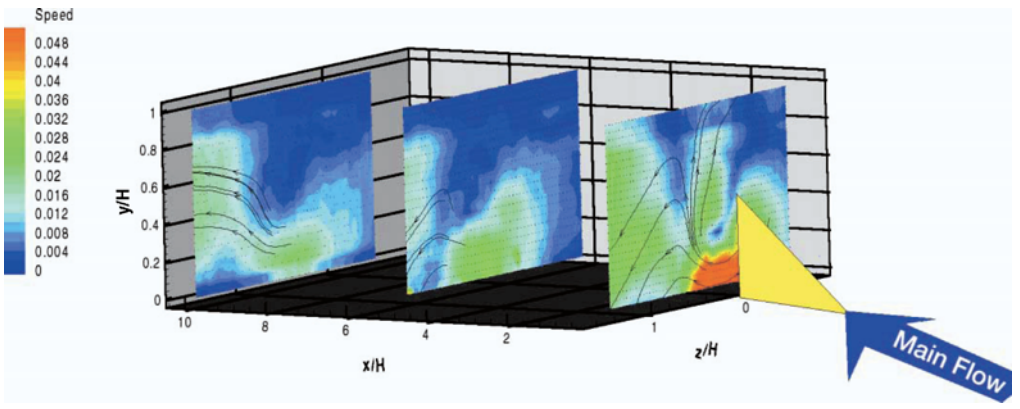

Fig. 7. Velocity profiles along atreamwise direction (CTAC30 and Re = 20,000).

In order to visualize the development of the generated longitudinal vortex under drag reduction conditions more in detail, the contours of vorticity, w, at the streamwise locations, x/H = 1, 3, 5 and 10 were plotted in Fig. 8, together with the streamlines. The vorticity, w, was defined as Eq. (2). The concentration of CTAC was 100 ppm, and the Reynolds number was fixed at Re = 4,500.

$$w = \frac{\partial v}{\partial z} - \frac{\partial w}{\partial y} \tag{2}$$

In these vorticity contours, the main flow direction is out of the paper plane, facing upstream, and a schematic drawing of the WVG was also made with dashed lines. It is clearly seen that the vorticities in the main flow surrounding the vortex are remarkably depressed, compared with the water case. The vorticity in the vortex core region, on the other hand, shows its maximum, and slowly decays along the streamwise direction. The rotation of the vortex was found anti-clockwise, looking upstream, regardless of the surfactant concentration. It is

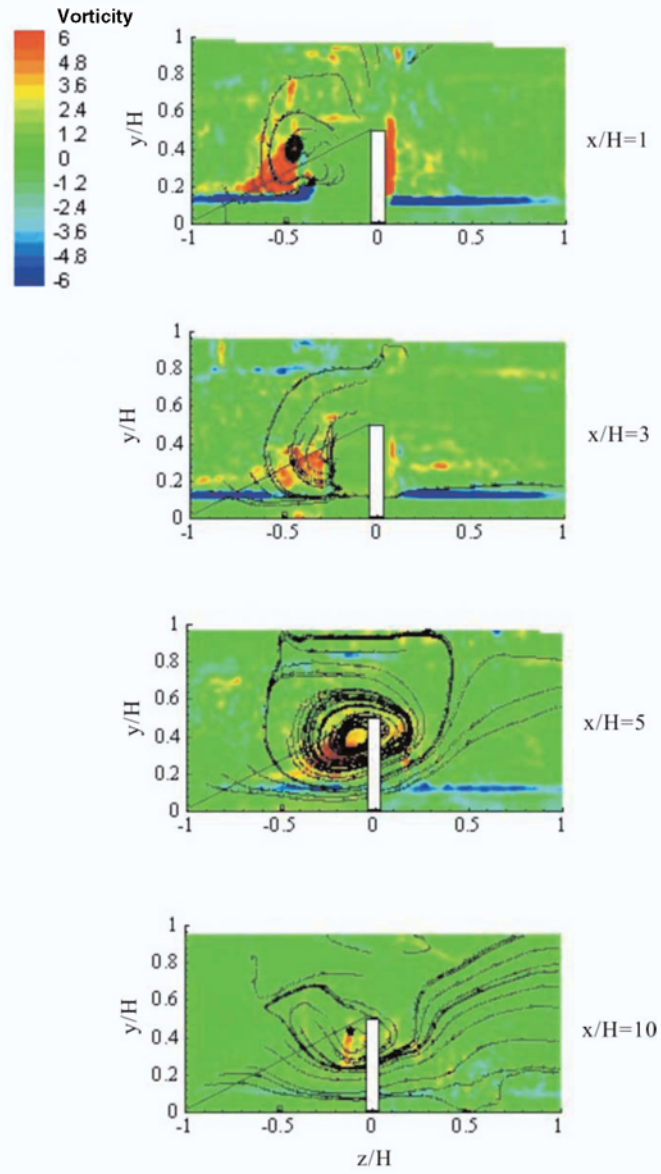

Fig. 8. Vorticity contours (y-z section, *Re* = 4,500 and CTAC100).

also seen in the streamline patterns of the figure that the vortex grows up along the streamwise direction to $x/H = 3$. The center of the vortex moves in y-direction towards the channel center to stabilize the vortex itself, but the ceiling of the channel limits the growth of the vortex. The vortex gets weaken and gradually vague in the range $x/H > 3$.

Different cross-sectional vorticity contours at $y/H = 0.24$, viewing from the top, are shown in Figs. 9 and 10, the Reynolds numbers of which are, respectively, $Re = 4{,}500$ and 9,900 under the same surfactant concentration, 30ppm. As observed easily in Fig. 9, the regions influenced by the longitudinal vortex are very limited approximately from $z/H = -0.5$ to $z/H = 1$. Here, the vortical streaks are rather slim in contrast to the case visualized in Fig. 10. The vorticity distribution appears clearly to be well ordered with negative vorticity regions on the positive z/H side, and positive ones on the negative z/H side. Also, the streamlines drawn in Fig. 9 show remarkably smooth paths even in the vortex core, whereas in Fig. 10, the streamlines are squeezed together and forced outside toward the positive z/H direction.

The vorticity distribution in Fig. 10 has no clear structures and shows the mixing-up of positive and negative regions of the vorticity. Big difference between the vorticity patterns in Figs. 9 and 10 demonstrates that the flow conditions change dramatically due to locally high shear rates with the increase of Reynolds. This shear-introduced phenomenon was observed in other experimental studies (Tiggelbeck et al., 1993; Kawaguchi et al., 1997). In the case of $Re = 9{,}900$, the flow has high shear rates over a critical shear rate, and locally recovers to the

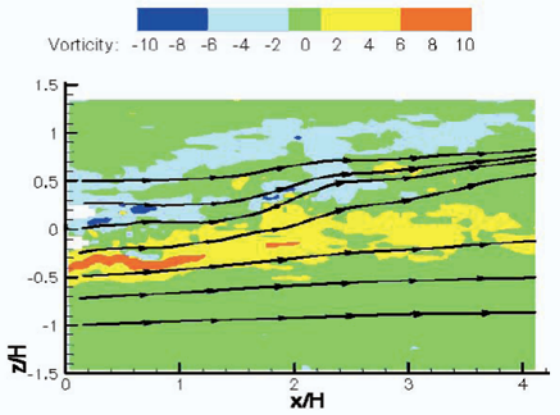

Fig. 9. Vorticity contours (x-z section, $y/H = 0.24$ CTAC30 and $Re = 4{,}500$).

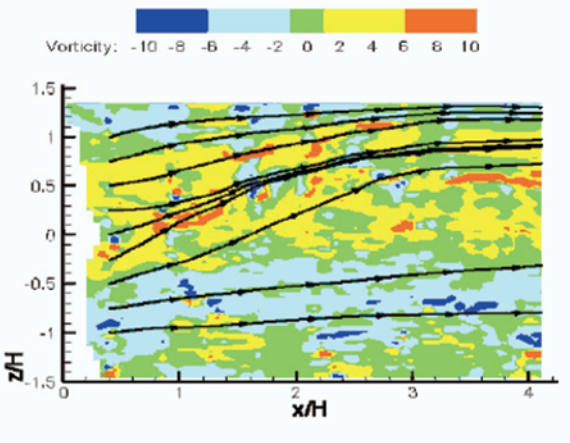

Fig. 10. Vorticity contours (x-z section, $y/H = 0.24$, CTAC30 and $Re = 9{,}900$).

solvent turbulent flow conditions due to intense vortical motions. High shear flows may cause the internal alignment of the micelles to break, and then the fluid properties recover to the values of the pure solvent, water.

4. Conclusions

The flow visualization of a longitudinal vortex behind the WVG in drag-reducing flows was made by means of fluorescent dye video capture and PIV measurement under the four CTAC/NaSal surfactant concentrations, 0 ppm, 30 ppm, 100 ppm and 200 ppm in the Reynolds number ranges, $2 \times 10^3 \sim 2 \times 10^4$. The results obtained in the present study are summarized as follows:

(1) Under the drag-reduction conditions, the mass and momentum transfer is remarkably suppressed and the growth of the vortex scale is limited, compared with the water case.
(2) The flow and vortical structure of CTAC/NaSal solution strongly depend on the surfactant concentration and Reynolds number. Concerning the vorticity distribution in the drag reduction cases, in particular, the distribution patterns show regular and well ordered, compared with the non-drag reduction cases.
(3) Under the drag-reducing flow conditions, the longitudinal vortex remains in a long streamwise distance downstream of the WVG and stabilizes in the center of the channel.
(4) The damped turbulence in the drag-reducing flows is recovered with locally high shear rate flows generated behind the WVG. At those locations where the shear stress exceeds the surfactant concentration specific critical value, the micelle effect can be neglected and drag-reducing flow properties are changing towards the ones of the pure solution, water.

Acknowledgments

The authors will express their gratitude to "Deutscher Akademischer Austauschdienst (DAAD)" for supporting the present experimental study.

References

Eschenbacher, J. F., Joko, M., Nakabe, K. and Suzuki, K., Visualization of Drag Reducing Flow Disturbed by a Vortex Generator, Proceeding of the 36th National Heat Transfer Symposium of Japan (Kumamoto, Japan), (1999), Vol. 3, 549-550.

Eschenbacher, J. F., Joko, M., Nakabe, K., and Suzuki, K., Characteristics of Longitudinal Vortices Generated in Drag-reducing Flows, to appear in International Journal of Transport Phenomena (2001).

Gyr, A. and Bewersdorff, H. W., Drag Reduction of Turbulent Flows by Additives, (1995), 5-6, Kluwer Academic Publisher, Dodtrecht, Netherlands.

Kawaguchi, Y., Daisaka, H., Yabe, A., Hishida, K. and Maeda, M., Turbulent Characteristics in Transition Region of Dilute Surfactant Drag Reducing Flows, Proceedings of the 11th Symposium on Turbulent Shear Flows (Grenoble, France), (1997), Vol. 1, P1-49-P1-54.

Tiggelbeck, St., Mitra, N. K. and Fiebig, M., Experimental Investigations of Heat Transfer Enhancement and Flow Losses in a Channel with Double Rows of Longitudinal Vortex Generators, Int. J. Heat and Mass Transfer, 26-9 (1993), 2327-2337.

Virk, P. S., Mickely, H. S. and Smith, K. A., The Ultimate Asymptote and Mean Flow Structure in Toms' Phenomenon, Trans. ASME ; Journal of Applied Mechanics, 37-2 (1970), 488-493.

Author Profile

Jens F. Eschenbacher: He graduated from the Process Engineering Department, the Friedrich-Alexander-University in Erlangen, Germany, in 1996 as "Diplom Ingenieur" under Professor. F. Durst's supervision. After his graduation, he went to Japan, and enrolled in "International Course" of Mechanical Engineering Department, Kyoto University and then in Doctoral Course of the same department. His research interest in Mechanical Engineering is particularly based on fluid mechanics and heat transfer including Non-Newtonian fluids.

Kazuyoshi Nakabe: He graduated from the Department of Mechanical Engineering, Kyoto University, in 1981, and received his Master degree of Mechanical Engineering in 1983 from Graduate School of Kyoto University. He received his Doctoral degree in 1991 from Graduate School of Osaka University while working as a research associate there before taking up his current position as an associate professor at Kyoto University. His research interests are in the fields of turbulent mixing, heat transfer and combustion.

Kenjiro Suzuki: He graduated from the Department of Mechanical Engineering, Kyoto University in 1962. After working at Kobe Steel Ltd. for one year, he returned to Department of Mechanical Engineering, Kyoto University, as Instructor and received his Doctoral degree in 1972. He was promoted to Associate Professor of the same department in 1975, and to Professor in 1986. He took up Russel Severance Springer Professor of the University of California, Berkeley, US, Invited Professor of the Institute National Polytechnique de Grenoble, France, and Invited Professor of Buergers Center, Delft University of Technology, Netherlands. He was formally the president, Japan Society of Heat Transfer. His research topics are mainly on unsteady or turbulent flows and related heat transfer with both numerical and experimental approaches including micro heat transfer and energy distributed system with micro gas turbine.